Vibrational Spectra of Nickel and Platinum Dioxide Molecules Isolated in Solid Argon

Delphine Danset,[†] Laurent Manceron,*[,†] and Lester Andrews[‡]

LADIR/Spectrochimie Moléculaire CNRS UMR 7075, Université Pierre et Marie Curie, case 49, 4 place Jussieu 75252 Paris, France, Department of Chemistry, University of Virginia, Box 400319, Charlottesville, Virginia 22901-4319

Received: February 15, 2001; In Final Form: May 22, 2001

The reactions of two group 10 metal atoms, nickel and platinum, with oxygen molecules at low temperature in solid argon have been reinvestigated. New information has been gathered on the interactions between transition metals and oxygen, more precisely, on platinum and nickel superoxides and their insertion products. For $Pt(O_2)$ the low-frequency metal−ligand ν_2 and ν_3 fundamentals have been observed and derived harmonic potential constants are compared to those of $Ni(O_2)$. Interest will then be taken in the dioxide insertion products, their differences in bonding as well as their production mechanisms. The positions of all three fundamentals for OPtO and of the two IR-active vibrations for ONiO have been experimentally determined and are compared to recent ab initio predictions.

Introduction

Despite their importance in material or surface science and in catalysis, our knowledge of the basic properties of simple group 10 transition metal (TM) molecules is still limited. One of the characteristics of the metal oxide molecules is the presence of several states in the ground-state vicinity, arising from different occupations of the highest energy σ or π molecular orbitals.[1] Several recent theoretical studies have been devoted to predictions of ground-state electronic and geometrical properties using various quantum mechanical methods.[2−4] Due to the difficulty of generating high densities of these reactive molecules, experimental studies have been relatively few. Gas-phase reaction kinetics studies of Ni atoms and O_2 molecules give thermochemical data,[5] and photodetachment electron spectroscopy (PES) of jet-cooled nickel mono-, di-, and superoxide species yielded electronic energy spacings and electron affinities along with an estimate of the vibrational frequency for the symmetrical NiO stretching mode (ν_1) in the ONiO molecule.[6]

Matrix isolation IR spectroscopic analysis of the reaction products from the co-condensation of the metal + O_2 reaction product in solid rare gases is a powerful technique for studying these reactive molecules and their formation pathways. In an earlier study, Huber and co-workers[7] applied this technique to group 10 TM atoms. The study was based on the O−O stretching frequencies and were thus limited to general trends in bonding in superoxides and disuperoxides $M(O_2)$ and $M(O_2)_2$ with M = Ni, Pd, Pt. More recently, reactions of these TM atoms produced by laser ablation with oxygen molecules diluted in solid argon have been investigated.[8,9] The elusive nickel and platinum dioxide molecules (ONiO, OPtO) were characterized through their metal−oxygen antisymmetrical vibrations (ν_3). This constitutes a powerful technique to generate and trap a variety of products. Since the ablation process produces metal atoms, photons up to the UV range and charged species, it has been successfully applied to the production of neutral and charged oxide molecules.[10] One of the main objectives in these studies is to provide complete sets of experimental data, to serve in databases or to test the performances of various quantum-mechanical methods. Although laser ablation is very useful in producing a whole array of neutral and charged metal oxide species, it is difficult to preferentially scale-up the quantity of the neutral compounds while limiting the production of these charged species. As a result this makes the detection of weak IR bands difficult. This study thus presents a reinvestigation of the reaction of ground-state Ni and Pt atoms and molecular oxygen in solid argon. We present here new material detailing the photochemical process leading to the metal dioxide molecules and supplementing their infrared spectra.

Experimental Section

The experimental procedures are the same as those described in ref 11. $Ni(O_2)$ and $Pt(O_2)$ molecules were prepared by co-condensing Pt or Ni vapor and dilute O_2−Ar mixtures (1−4% O_2 in Ar), onto a flat, highly polished, Ni-plated copper mirror maintained at less than 10 K using a closed-cycle cryogenerator, situated in a stainless steel cell evacuated to a base pressure of about 10^{-7} mbar before refrigeration of the sample holder. The furnace enclosed the metal atom source inside a liquid nitrogen-cooled assembly, thereby minimizing greatly the amount of outgassing impurities caused by the elevated temperature of the metal source. A tungsten filament, wetted with Pt (Ni), was heated from 1700°−2000 °C (1300°−1500 °C) to generate the metal vapor. The metal deposition rate was carefully monitored with the aid of a quartz microbalance and was typically of the order of about 10^{-6} mol/hour.

High-purity argon (Air Liquide, France; 99.995%) and $^{16}O_2$ (Air Liquide, France; 99.998%) and $^{18}O_2$ (Isotec, USA, 99.0% ^{18}O), were used to prepare the O_2−Ar mixtures. To prepare scrambled oxygen ($^{16}O^{18}O$), equal quantities of $^{16}O_2$ and $^{18}O_2$ were mixed and submitted to a Tesla discharge for approximately 10 min, yielding a 25% $^{16}O_2$, 50% $^{16}O^{18}O$, and 25% $^{18}O_2$ mixture.

In general, after depositing metal and gas for 45−90 min, infrared spectra of the resulting sample were recorded in the transmission-reflection mode between 5000 and 80 cm^{-1} using a Bruker 120 FTIR spectrometer and the appropriate combinations of KBr/Ge, or 6 μm Mylar beam splitters with either liquid N_2-cooled narrow band InSb or HgCdTe photodiodes, or a liquid

* To whom correspondence should be addressed. E-mail: lm@ccr.jussicn.fr.
† Université Pierre et Marie Curie.
‡ University of Virginia.

10.1021/jp010605x CCC: $20.00
Published on Web 07/11/2001

He-cooled Si−B bolometer fitted with cooled band-pass filters. The resolution was varied from 0.5 to 0.05 cm^{-1}. Also, absorption spectra in the near-, mid-, and far-infrared were collected on the same samples through either CsI or polyethylene windows mounted on a rotatable flange separating the interferometer vacuum (10^{-2} mbar) from that of the cryostatic cell (10^{-7} mbar). Bare mirror backgrounds, recorded at 10 K from 5000 to 70 cm^{-1} prior to sample deposition, were used as references in processing the sample spectra. The spectra were subsequently subjected to baseline correction to compensate for infrared light scattering and interference patterns.

The IR intensity measurements for the Pt + O_2 samples required special attention, because the absorptions were very weak in near- and far-IR domains and stronger in the mid-IR PtO fundamental regions. Furthermore, numerous bands were observed for linear OPtO and assumed to be different sites within the matrix. To study these effects properly, care was taken first to make measurements on the same samples in the various spectral ranges; second, to repeat these measures on both optically thick and thin samples to limit the photometric errors; and last, to use the band decomposition procedure to estimate relative intensities for partially overlapping bands.

The sample was irradiated for 30 min at 580 nm using a 200 W mercury−xenon high-pressure arc lamp and an interference filter centered on the 580 nm wavelength and then irradiated for another 30 min in the UV region using a 420−200 nm band-pass filter. The last step entailed annealing the sample to 20 K, by shutting off the cryogenerator. Once the desired temperature was reached, the sample was recooled to 10 K by reactivating the cryogenerator, and then the spectra were seconded. Infrared spectra of the photolyzed and annealed samples were recorded between 5000 and 80 cm^{-1}, as outlined above.

For the Ni + O_2 samples, attention was focused on the absorption bands of linear ONiO in the mid- and far-infrared regions. The sample was submitted to broad-band irradiation using a 200 W mercury−xenon high-pressure arc lamp. A more detailed photolysis, using filters centered on the intense Hg emission lines at 334, 313, 289, and 265 nm, was carried out, to study the rearrangement $Ni(O_2) + h\nu \rightarrow ONiO$. The same care and precautions were taken in recording the IR spectra of the nickel system as those taken for the platinum.

Results

Pt + O_2. The co-condensation of the thermally evaporated Pt atoms and the O_2−Ar mixture (1−4%) at 10 K, produced essentially $Pt(O_2)$ (superoxide), the insertion product, OPtO, and some $Pt(O_2)_2$ species in sharply increasing amounts when the oxygen concentration was raised. In an earlier study Andrews and co-workers[9] have assigned the band at 928.1 cm^{-1} to the ν_1 (O−O stretch) of the superoxide and the sharp band at 961.7 cm^{-1} and larger multiplet around 953.4 cm^{-1} to ν_3 (antisymmetric stretch) of OPtO. The presence of these two different peaks for the same vibration was attributed to a trapping site effect, the sharp peak labeled as "site 1" and the broader one as "site 2", both containing OPtO molecules in slightly different argon packing arrangements (Figure 1).

After deposition, the main product is $Pt(O_2)$, along with a small amount of OPtO. In the lower mid- infrared region the two absorption bands observed at 512.3 and 551.2 cm^{-1}, correlate with the 928.1 cm^{-1} band on both Pt and O_2 concentration changes. These bands disappeared upon photolysis at 580 nm and reappeared after annealing to 20 K, tracking the absorbance of the $Pt(O_2)$ 928.1 cm^{-1} band.

Formation of the OPtO molecule was induced by two distinct photochemical processes, which turned out to be site selective.

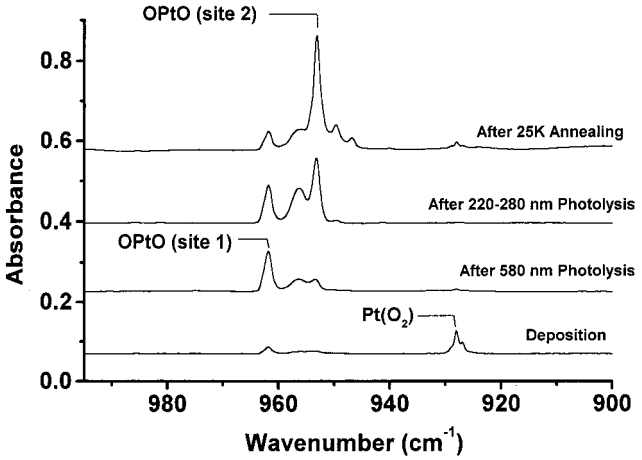

Figure 1. Infrared spectra in the 990−900 cm^{-1} region for thermally evaporated Pt atoms co-deposited with 1% O_2 in argon.

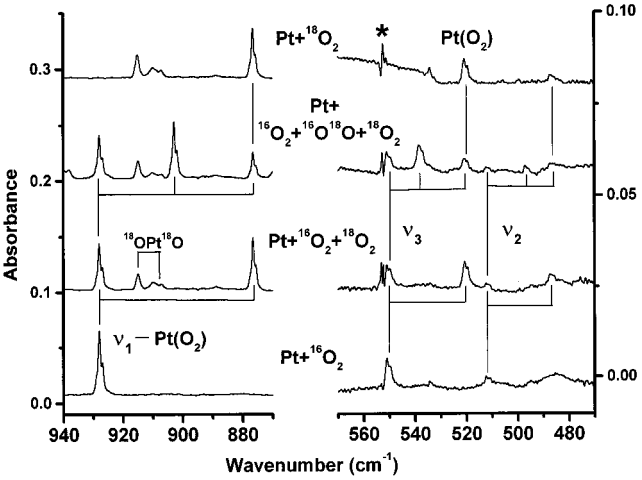

Figure 2. Infrared spectra in the 940−870 and 570−470 cm^{-1} regions for thermally evaporated Pt atoms co-deposited with 1% O_2 in argon using various isotopic precursors. The asterisk designates an instrumental artifact.

First, irradiation of the sample with 580 nm light favored the formation of OPtO in site 1, with only a minor quantity being trapped in site 2. In addition, the photolysis resulted in the destruction of $Pt(O_2)$. The second irradiation, in the UV region was "site-2-selective" causing a marked growth of the multiplet centered at 953.4 cm^{-1}. A band at 157.2 cm^{-1} in the far-infrared was observed to follow this same pattern. Finally, two weaker bands were observed at 1856.9 and 1838 cm^{-1}. Their behaviors were not completely alike, the band at 1856.9 cm^{-1} grew noticeably with 580 nm photolysis, only to decrease after annealing, whereas the band at 1838.0 cm^{-1} was unaffected by the 580 nm irradiation but grew after the UV photolysis and sharpened after annealing. They are therefore associated with the OPtO product, evolving like the 953.4 and 961.7 cm^{-1} bands, sites 1 and 2, respectively.

Further evidence is provided by the isotopic effects (Figure 2, Table 1). When replacing $^{16}O_2$ by $^{18}O_2$, the bands observed at 512.3 and 551.2 cm^{-1} for $Pt(O_2)$ shifted respectively to 487.3 and 520.7 cm^{-1}. As for OPtO, both sites shifted equally to 914.8 and 909.9 cm^{-1}. The band observed at 157.2 cm^{-1} shifts to 149.6 cm^{-1}, while the weaker bands at 1800 cm^{-1} were shifted to 1759.8 and 1742.2 cm^{-1} respectively (Figure 3). Besides the bands due to $^{16}OPt^{16}O$ and $^{18}OPt^{18}O$, a significant number of new signals appear in the IR spectrum for the reaction between Pt and the $^{16}O_2 + {}^{18}O^{16}O + {}^{18}O_2$ isotopic mixture, and are thus

TABLE 1: Vibrational Frequencies (cm^{-1}) and Relative Intensities (in Parentheses) of the IR Absorption Bands for Various Pt + O_2 Reaction Products Observed in Solid Argon

assignment	Pt + $^{16}O_2$	Pt + $^{18}O_2$	Pt + $^{16}O^{18}O$[a]
Pt(O_2) ν_1	928.1 (1)	876.4 (1)	903.0 (1)
ν_2	512.3 (0.05)	487.3 (0.08)	497.2 (0.02)
ν_3	551.2 (0.22)	520.7 (0.24)	538.5 (0.35)
OPtO (site 1) ν_1			870.0 (0.1)
ν_3	961.7 (1)	914.8 (1)	947.2 (1)
$\nu_1 + \nu_3$	1856.9 (0.03)	1759.8 (0.02)	$\approx$1810.7 $\pm$ 0.3[b]
OPtO(site 2) ν_1			861.9, 860.1 (0.1)
ν_2	157.2 (0.04)	149.6 (0.03)	153.3 (0.04)
$O^{194}PtO$ ν_3	953.39[c] (1)	909.9[d] (1)	938.0, 939.3[e] (1)
$O^{195}PtO$	953.06[c]		
$O^{196}PtO$	952.71[c]		
$O^{198}PtO$	952.04[c]		
$\nu_1 + \nu_3$	1838.0 (0.01)	1742.2 (0.01)	1793.1 (0.005)
OPtO(site 3) ν_3	956.4	941.1	906.8

[a] In $^{16}O_2$ + $^{16}O^{18}O$ + $^{18}O_2$ mixture. [b] Uncertain frequency due to overlapping. [c] Measured with 0.05 cm^{-1} resolution. [d] Center of multiplet. [e] Split by matrix interaction; collapsing reversibly at 25 K into a single component at 939.1 cm^{-1}.

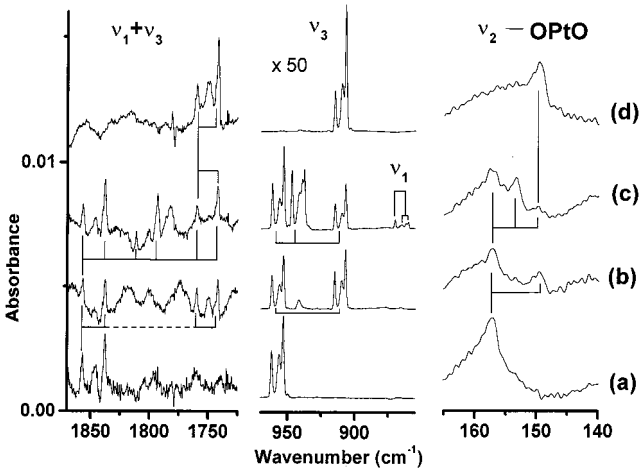

Figure 3. Infrared spectra in the 1860−1740, 940−870, and 570−470 cm^{-1} regions for Pt atoms co-deposited with 1% O_2 in argon using various isotopic precursors, after 220−280 nm light excitation and annealing to about 25 K: (a) Pt + $^{16}O_2$; (b) Pt + $^{16}O_2$ + $^{18}O_2$; (c) Pt + $^{16}O_2$ +$^{16}O^{18}O$ + $^{18}O_2$; (d) Pt + $^{18}O_2$.

due to the Pt + $^{18}O^{16}O$ reaction product. In the far-infrared, an intermediate peak at 153.3 cm^{-1} appears upon photolysis. In the mid infrared, a sharp band appears at 870.0 cm^{-1}, which grows upon 580 nm photolysis and decreases after annealing. Like the 947.2 cm^{-1} absorption band, which is associated with $^{16}OPt^{18}O$ (ν_3, site 1), the 870.0 cm^{-1} band only appears in the presence of $^{18}O^{16}O$ precursor and therefore belongs to $^{18}OPt^{16}O$. In addition, a broader band grows upon UV photolysis around 860.0 cm^{-1}, sharpening after annealing and behaving like the absorption bands at 938.0 and 939.3 cm^{-1}, corresponding to site 2 of the $^{16}OPt^{18}O$ insertion product. The isotopic effects for the ν_3 fundamental of OPtO are somewhat complex. Indeed, two interesting effects have been observed. The first is an extra shoulder at 939.3 cm^{-1} in the site 2 multiplet for the $^{16}O_2$ + $^{18}O^{16}O$ + $^{18}O_2$ precursor, placed between the expected bands at 941.6 and 938.0 cm^{-1}. The second is the presence of an absorption band at 941.8 cm^{-1}, which upon annealing to about 29 K and recooling to 9 K is transformed into the doublet at 939.3 and 938.0 cm^{-1}. Upon warming the argon matrix to about 22 K, this structure observed specifically with the $^{18}O^{16}O$ precursor collapses back to a single band at 939.1 cm^{-1} (spectrum taken at 22 K).

Interest was also taken in the isotopic shifts due to the natural abundance of Pt. A high-resolution spectrum (0.05 cm^{-1}) in the mid-infrared region is presented on the ν_3 fundamental of OPtO after annealing the sample to 20 K to decrease the spectral line widths and allow OPtO to diffuse to the most stable trapping site, site 2. The experimental spectrum is presented on Figure 4 and compared to a simulation produced with four components at 953.39, 953.06, 952.71, and 952.04 cm^{-1}, to which were given the statistical weights of the ^{194}Pt, ^{195}Pt, ^{196}Pt, and ^{198}Pt isotopes of platinum and Lorentzian band shapes with 0.25 cm^{-1} full width at half-maximum. This also confirms the presence of only one Pt atom in this molecule.

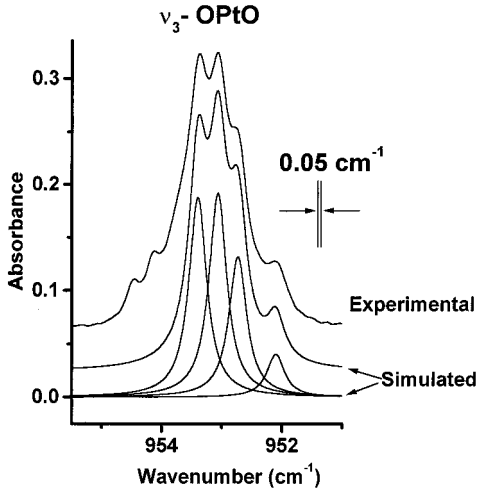

Figure 4. Comparison of high-resolution Infrared spectrum in the ν_3 region of OPtO (site 2) for Pt + $^{16}O_2$ in argon after UV excitation and annealing to 25 K, and simulations based on the ^{194}Pt, ^{195}Pt, ^{196}Pt, and ^{198}Pt isotopes of platinum and Lorenzian band shapes with 0.25 cm^{-1} full width at half-maximum.

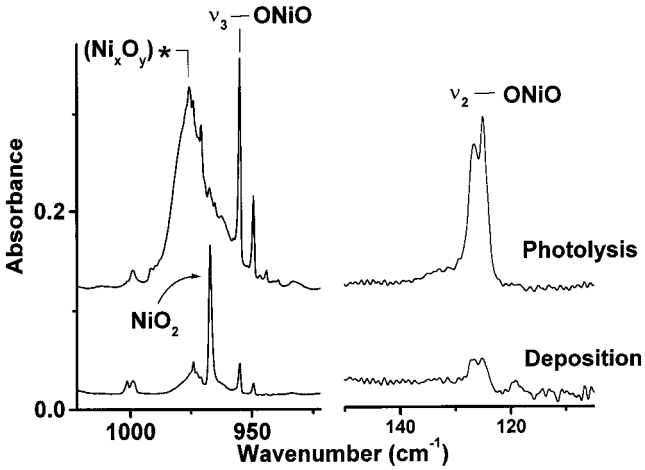

Figure 5. Infrared spectra in the 1025−920 and 150−100 cm^{-1} regions for thermally evaporated Ni atoms co-deposited with 1% O_2 in argon after deposition (bottom) and 200−400 nm light excitation (top). The asterisk designates a larger stoichiometry aggregate (likely Ni_2O_2, see ref 8).

Ni + O_2. In a prior study involving nickel oxide complexes in solid argon matrices, Andrews and co-workers[8] characterized the superoxide Ni(O_2) in a complete matter, as well as the ν_3 fundamental of the ONiO insertion product. Later, Wu and Wang[6] placed the ν_1 fundamental of ONiO around 750 $\pm$ 30 cm^{-1} by photoelectron spectroscopy in the gas phase.

Figure 5 presents the main products following deposition and broad-band UV−visible irradiation. The Ni(O_2) superoxide, characterized by the band at 967.1 cm^{-1}, is the abundant product after deposition. A small amount of ONiO, characterized by its ν_3 absorption at 954.9 and 949.3 cm^{-1} (doublet due to the ^{58}Ni

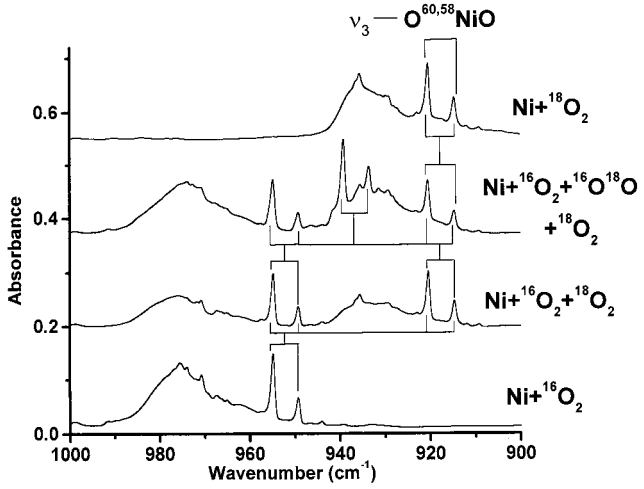

Figure 6. Infrared spectra in the 1000−900 cm^{-1} region for Ni atoms co-deposited with 1% O_2 in argon using various isotopic precursors, after 200−400 nm photolysis.

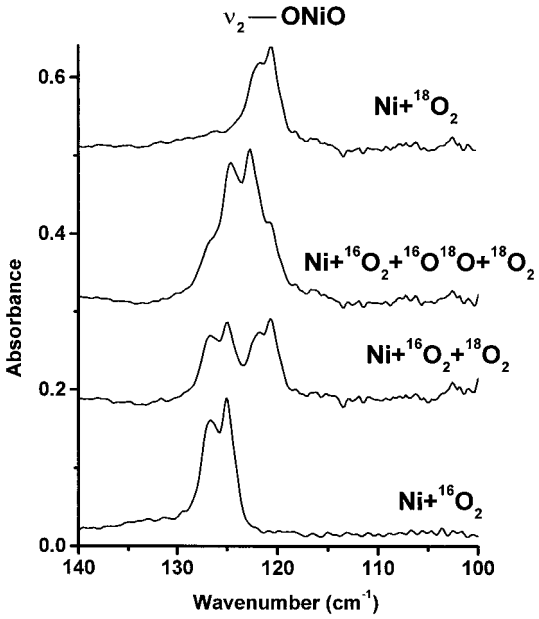

Figure 7. Infrared spectra in the 140−100 cm^{-1} region for Ni atoms co-deposited with 1% O_2 in argon using various isotopic precursors, after 200−400 nm light excitation.

and ^{60}Ni isotopes in natural abundance), was also detected. After photolysis, this trend reverses: Ni(O_2) disappears and the ONiO band markedly grows.The large broad band at 980 cm^{-1}, previously assigned to a (Ni_2O_2) species,[8] presents a higher order dependence on Ni. As this species is not the object of our study, it will not be discussed further. However, the growth of a strong band at 125 cm^{-1} after photolysis is of interest. This bands common behavior with the ν_3 fundamental of ONiO, during photolysis or with concentration effects, indicates that it belongs to ONiO. Again, further evidence for the attribution of the band is provided by isotopic substitution. The triplet structure observed for the ν_3 fundamental of ONiO (Figure 6) shows the type of isotopic structure expected for the other bands belonging to this species. With $^{16}O_2$ + $^{18}O^{16}O$ + $^{18}O_2$, a triplet structure is observed for the band at 125.0 cm^{-1}, shifting to 122.7 cm^{-1} with the $^{16}O^{18}O$ precursor and 120.5 cm^{-1} with $^{18}O_2$, as shown in Figure 7. This observation confirms that the 125.0 cm^{-1} band belongs to ONiO.

The photolysis study of the Ni + O_2 reaction products consisted of three irradiations at different monochromatic

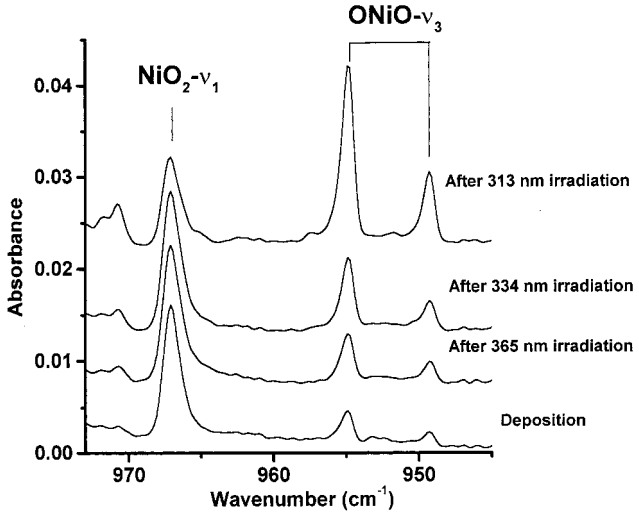

Figure 8. Infrared spectra in the 940−980 cm^{-1} region for Ni atoms co-deposited with 1% O_2 in argon after irradiation with different wavelengths.

wavelengths, during which attention was focused on the relative behavior of the ONiO and Ni(O_2) bands. Irradiation at 365 nm shows the growth of both species (Figure 8), whereas at 334 nm causes the ONiO band to grow while the Ni(O_2) band is left unchanged. Last, the irradiation at 313 nm shows an antiparallel evolution, where the ONiO band is multiplied almost by 3, and the band for Ni(O_2) is reduced by half.

Discussion

New information has been gathered on the interactions between Ni and Pt atoms and oxygen, more precisely, on platinum and nickel superoxides and their insertion products. After discussing briefly the mechanisms for their formation, complementary data on Pt(O_2) will be discussed and compared to that for Ni(O_2). Finally, interest will be taken in the Pt and Ni insertion products, their differences in structure, bonding, and behavior.

Production Mechanisms. With Pt atoms, our results clearly indicate two possible reaction pathways. First, reaction of ground-state Pt with O_2 leads to the superoxide complex which then, upon electronic excitation with moderate energy (2.65 eV), rearranges to the dioxide insertion product. The second possible reaction pathway, requires more energetic UV light in the 5.5−6 eV range corresponding to the $5d^9\ 6s^1 \rightarrow 5d^9\ 6p^1$ atomic Pt excitations[12] and causes no loss of IR-absorbing precursor. The second pathway is thus likely to be diffusion and reaction of excited-state Pt atoms under irradiation with nonadjacent O_2 molecules. Note that each of these two pathways lead to dioxide insertion products formed in a slightly different environment. For instance, the first generates OPtO molecules in the argon cage of the superoxide precursor, which are slightly more constrained than those formed after atomic excitation and diffusion (compare the "site 1" and "site 2" ν_1 or ν_3 absorptions). We note that in solid neon two sharp bands were observed for OPtO at 958.7 and 950.5 cm^{-1}, supporting the matrix site model.[13] The results with Ni are slightly more complex to analyze because the nickel superoxide electronic transitions are shifted to higher energy (about 4.1 eV) in a region overlapping partially the Ni atomic lines. Our results show that UV light near 310 nm causes the Ni(O_2) → ONiO insertion reaction to occur and that the superoxide species is not the only reservoir for the production of the dioxide insertion product. As with Pt atoms, excitation in the UV range (350−330 nm, for instance),

TABLE 2: Vibrational Frequencies[a] and Relative Intensities (in Parentheses) of the IR Absorption Bands for Various Ni + O_2 Reaction Products Observed in Solid Argon

assignment	Ni + $^{16}O_2$	Ni + $^{18}O_2$	Ni + $^{16}O^{18}O$[b]
$^{58}Ni(O_2)$ ν_1	967.1 (1)	914.5 (1)	941.3 (1)
ν_2	538.3 (0.07)	518.8 (0.03)	530.2 (0.40)
ν_3	511.7 (0.40)	485.7 (0.40)	496.3 (0.02)
$^{60}Ni(O_2)$ ν_2	535.3 (0.05)	516.1 (0.01)	
ν_3	510.9		
$O^{58}NiO$ ν_2	125.0 (1)	120.6 (1)	122.7 (1)
ν_3	954.9 (0.72)	920.4 (0.73)	939.2 (0.82)
$O^{60}NiO$ ν_3	949.3 (0.27)	914.7 (0.25)	933.6 (0.40)

[a] Vibrational frequencies in cm^{-1}. The values quoted are within ± 0.1 cm^{-1}. [b] In $^{16}O_2 + {}^{16}O^{18}O + {}^{18}O_2$ mixture.

TABLE 3: Comparison of the Experimental Frequencies and Calculated[a] Harmonic Frequencies (cm^{-1}) for the Various Isotopic Species of PtO_2

	$^{194}Pt^{16}O_2$		$^{194}Pt^{18}O_2$		$^{194}Pt^{16}O^{18}O$	
species	exp	calc	exp	calc	exp	calc
ν_1	928.1	928.6	876.4	875.5	903.0	902.7
ν_2	512.3	512.2	487.3	487.1	497.2	496.0
ν_3	551.2	551.2	520.7	520.5	538.5	539.2

[a] The force constants giving the best fit of the experimental data are $F_{PtO} = 2.70$ mdyn $Å^{-1}$, $F_{OO} = 3.97$ mdyn $Å^{-1}$, $F_{PtO,PtO} = -0.92$ mdyn $Å^{-1}$, $F_{PtO,OO} = -0.196$ mdyn $Å^{-1}$, and $\theta_{OPtO} = 47°$.

where $3d^9\ 4s^1 \rightarrow 3d^9\ 4p^1$ atomic transitions are found,[14] also causes formation of the dioxide insertion species, which can be interpreted with the same basic reaction pathways:

$$M + O_2 \rightarrow M(O_2)$$

$$M(O_2) + h\nu \rightarrow M(O_2)^*$$

$$M(O_2)^* \rightarrow OMO$$

Superoxides. Our results for $Pt(O_2)$ clearly showed three IR absorption bands, two of which had not been observed before. The bands at 551.2 and 512.3 cm^{-1} are assigned to the ν_3 and ν_2 fundamentals, respectively. The basis for their respective assignment lies in the magnitude of the observed isotopic shifts ($|\Delta\nu|$). The band at 551.2 cm^{-1} shifts to 520.7 cm^{-1} ($|\Delta\nu| =$ 30.5 cm^{-1}), and the band at 512.3 cm^{-1} shifts to 487.3 cm^{-1} ($|\Delta\nu| = 25.0$ cm^{-1}); the shift for the O−O stretch induces a $|\Delta\nu_1|$ of 50.1 cm^{-1}. The isotopic shift for this latter mode is close to that expected for a pure O−O stretching mode (about -53 cm^{-1}), indicating that the coupling of this coordinate with that of Pt−O is limited. With an acute OPtO bond angle, the contribution of Pt in the symmetric ν_2 vibration is accentuated while that of the oxygens is diminished. For the antisymmetric vibration, the contribution of Pt in the reduced mass decreases in favor of that of the oxygens, giving a larger isotopic shift. So the 512.3 cm^{-1} band corresponds to the symmetric vibration (ν_2) with the smaller isotopic shift, while the 551.2 cm^{-1} band corresponds to the antisymmetric Pt−O stretching (ν_3) with the larger shift. These assumptions have been tested using a semiempirical harmonic potential model and the results, presented in Table 3, fit the isotopic effects (within the usual limitations imposed by the neglect of anharmonicity), validating the proposed assignments. Former DFT calculations using the B3LYP functional, LanlD2Z effective core basis set for Pt and D-95* basis sets for oxygen predicted frequencies at 1065, 471, and 450 cm^{-1} for ν_1,ν_2, and ν_3, respectively. Comparison with the present results suggest a notable underestimation of the Pt−O interaction and of the O═O bond weakening, and an inversion of the two metal−ligand vibrational frequencies.

TABLE 4: Comparison of Experimental Frequencies and Calculated[a] Harmonic Frequencies (cm^{-1}) for the Various Isotopic Species of NiO_2

	$^{58}Ni^{16}O_2$		$^{60}Ni^{16}O_2$		$^{58}Ni^{18}O_2$		$^{58}Ni^{16}O^{18}O$	
species	exp	calcd	exp	calcd	exp	calcd	exp	calcd
ν_1	967.1	967.1	no[b]	966.7	914.5	913.3	941.3	940.8
ν_2	538.3	538.2	535.3	535.3	518.8	517.7	530.2	529.8
ν_3	511.7	511.7	510.9	510.7	485.7	485.7	496.3	496.5

[a] The force constants giving the best fit of the experimental data are $F_{NiO} = 2.43$ mdyn $Å^{-1}$, $F_{OO} = 3.76$ mdyn $Å^{-1}$, $F_{NiO,NiO} = -0.11$ mdyn $Å^{-1}$, $F_{NiO,OO} = -0.24$ mdyn $Å^{-1}$, and $\theta_{ONiO} = 57°$. [b] Not observed.

The $Ni(O_2)$ molecule has been characterized previously[8] and calculations using a harmonic force field similar to that presented above for $Pt(O_2)$ allows comparison of the bonding and interaction for the two superoxides, $Pt(O_2)$ and $Ni(O_2)$. Indeed, though these molecules have similar structures, the M−O and O−O force constants and their interaction constants significantly different. As shown in Tables 3 and 4, $F_{NiO} = 2.4$ mdyn $Å^{-1}$ and $F_{PtO} = 2.7$ mdyn $Å^{-1}$, making the PtO bond stronger than the NiO bond; both interaction constants are positive for $Ni(O_2)$, whereas they are negative for $Pt(O_2)$. This qualitative difference might be related to a switch in the electronic structure from triplet to singlet. Theoretical calculations done on $Ni(O_2)$ at the CASSCF[15] and, more recently, CCSD(T)[16] levels predicted a singlet ground state. All-electron DF calculations made more recently in order to predict the fundamental frequencies considered both triplet and singlet states.[8] The triplet state was found to be slightly lower in energy, but vibrational frequency predictions were quite different than what was in fact observed. While the O−O stretching frequency ν_1 was almost identical in both states, the metal−ligand motions, ν_2 and ν_3, were calculated around 516 and 60 cm^{-1} for the triplet state and 478 and 599 cm^{-1} for the singlet. Experimentally ν_2 has been assigned to the band at 538.3 cm^{-1} and ν_3 is observed at 511.7 cm^{-1} in solid argon. The difference between the experimental value of ν_2 and that calculated is larger for the triplet state than the singlet state, despite the fact that the triplet state possesses the largest binding energy and is therefore the ground state for these calculations. Calculations at a higher level of theory are thus needed on this species to determine the ground state in solid argon.

Finally, the NiOO, asymmetric superoxide, was not observed in these experiments. This species was suggested to appear on annealing to 20 K in the laser ablation experiments and its ν_1 fundamental observed at 1221.0 cm^{-1}. This band was not observed here after deposition, nor formed on annealing, which may result from the fact that thermal evaporation produces milder deposition conditions. This leads us to question the attribution or suppose that the species observed is obtainable only with Ni atoms from laser ablation, which are not directly accessible from our experimental conditions.

Insertion Products. This study brings new information to complete the characterization of both OPtO and ONiO molecules. For OPtO, the ν_2 fundamental and the ($\nu_1 + \nu_3$) combination bands have been observed around 157 and 1838 cm^{-1}, respectively. The ν_1 fundamental has also been observed for the asymmetrical isotopic species $^{16}OPt^{18}O$, near 861 cm^{-1}. The fact that the ($\nu_1 + \nu_3$) band is observed while ν_1 is inactive for OPtO is strong evidence that the molecule is linear. Further evidence is given by the good agreement between experimental frequencies and the frequencies and isotopic shifts calculated using a semiempirical harmonic potential assuming a linear structure (Table 5). The experimental data used for comparison

TABLE 5: Comparison of the Experimental Frequencies and Calculated[a] Harmonic Frequencies for the Various Isotopic Species of OPtO

	$^{16}O^{194}Pt^{16}O$		$^{18}O^{194}Pt^{18}O$		$^{18}O^{194}Pt^{16}O$		$^{16}O^{195}Pt^{16}O$		$^{16}O^{196}Pt^{16}O$		$^{16}O^{198}Pt^{16}O$	
species	exp	calc	exp	calc	exp	calc	exp	calc	exp	calc	exp	calc
site 2 $\nu_1(\Sigma_g^+)$	no[b]	892.4	no	841.3	861.9, 860.1	858.6	no	892.4	no		no	
ν_2 (Π_u)	157.2	157.2	149.6	149.3	153.3	153.4						
ν_3 (Σ_u^-)	953.4	954.0	909.9	907.4	938.0, 938.3	938.9	953.1	953.1	952.7	952.7	952.0	952.0
$\nu_1+\nu_3$[c]	1838.0	1839.9	1742.2	1742.2	1793.1	1796.1						

[a] The force constants giving the best fit of the experimental data are $F_{PtO} = 7.439$ mdyn Å^{-1}, $F_{PtO,\,PtO} = 0.068$ mdyn Å^{-1}, $F_{\theta\theta} \times r_{PtO}^{-2} \cong 0.10$ mdyn Å^{-1}, $\theta_{OPtO} = 180°$. [b] Not observed. [c] From the anharmonicity observed for $^{16}OPt^{16}O$, assuming a mass-dependent anharmonicity correction.

TABLE 6: Comparison of Experimental Frequencies and Calculated[a] Harmonic Frequencies (cm^{-1}) for the Various Isotopic Species of ONiO

	$^{16}O^{58}Ni^{16}O$		$^{16}O^{60}Ni^{16}O$		$^{18}O^{58}Ni^{18}O$		$^{16}O^{58}Ni^{18}O$	
species	exp	calc	exp	calc	exp	calc	exp	calc
ν_1 (Σ_g^+)	no[b]	728.0	no	728.0	no	687.3	no	706.7
ν_2 (Π_u)	125.0	125.0	no	124.3	120.6	120.6	122.7	122.7
ν_3 (Σ_u^-)	954.9	954.9	949.3	949.3	920.4	920.1	939.2	939.1

[a] The force constants giving the best fit of the experimental data are $F_{NiO} = 5.27$ mdyn Å^{-1}, $F_{NiO,NiO} = -0.27$ mdyn Å^{-1}, $F_{\theta\theta} r_{NiO}^{-2} = 0.047$ mdyn Å^{-1}, $\theta_{ONiO} = 180°$. [b] Not observed.

refer to site 2, the bending mode for site 1 remains either too weak to be detected or too close to that of site 1 to be resolved.

For nickel dioxide, the bending mode has been assigned to the band at 125.0 cm^{-1}. To compare the molecular parameters of ONiO and OPtO, semiempirical harmonic potential constants have been calculated for ONiO using the same procedure outlined above for OPtO again, assuming a linear geometry (Table 6). The frequency of the ν_1 mode was adjusted to reproduce best the asymmetry of the $^{16}ONi^{18}O$ (ν_3) frequency with respect to the average of the $^{16}ONi^{16}O$ and $^{18}ONi^{18}O$ values. The position of ν_1 estimated in this way (730 ± 20 cm^{-1}) is consistent with that established by PES in the gas phase 750 ± 30 cm^{-1} for this molecule, taking the error into account.[6] Unlike the case of OPtO, ν_1 was not observed for the asymmetrical $^{16}ONi^{18}O$ isotopic species. However, inspection of the eigenvectors calculated for both molecules shows that, in the hypothesis of a linear structure, the IR intensity ratio predicted between the two stretching modes $I\nu_1/I\nu_3 = 0.37\%$ in $^{16}ONi^{18}O$ and 9.6% in $^{16}OPt^{18}O$, consistent with what was in fact observed (Table 1). In principle, the linearity of the molecule could be discussed independently on the basis of the magnitude of the isotopic effects observed on ν_2, but given the ±0.2 cm^{-1} uncertainty on the measured frequencies, the bond angle can vary up to ±20° before the predicted isotopic shifts fall outside the error bars.

The comparison of the bending modes for these two species is quite interesting, indeed Pt being more than 3 times heavier than Ni, ν_2 of OPtO is be expected to be lower than that of ONiO, if the bonding is similar. Yet, it is the other way around, and the OPtO force constant is twice as large as that of ONiO, thereby making the molecule more rigid. This suggests either a better overlap of the Pt d-orbitals and the p-orbitals of the oxygens or a difference in electronic ground-state structures, which might not be firmly established. The PES results indirectly support a $^3\Sigma_g^-$ ground state.[6] However, DFT calculations suggest that the $^1\Sigma_g^+$ state is slightly lower in energy[8] but could not of course take spin−orbit coupling into account. The frequencies predicted for the singlet state at this level (805, 48, and 1027 cm^{-1} for ν_1, ν_2, and ν_3 respectively) are in relatively poor agreement (27% average deviation) with the values observed here in solid argon, however. Clearly, more work is needed to describe the ground state of these molecules.

The comparison of the metal−oxygen bond force constants in the di- and triatomics is also of interest. In the case of the NiO bond, $F_{NiO} = 5.0$ mdyn Å^{-1} for the diatomics and $F_{NiO} = 5.27$ mdyn Å^{-1} for ONiO, whereas for the PtO bond, $F_{PtO} = 5.9$ mdyn Å^{-1} for PtO and $F_{PtO} = 7.4$ mdyn Å^{-1} for OPtO. In both instances the metal−oxygen bond is reinforced in going from the diatomic to the triatomic. However, in the case of the PtO bond a much stronger reinforcement occurs, a paradoxical result given the positive sign of the $F_{PtO,PtO}$ interaction constant found for OPtO. This indicates a cooperative effect on the O atom bonding to the metal center, comparable to that observed for some transition metal carbonyls such as $Fe(CO)_n$, $n = 1-4$, where the carbonyl dissociation energies per bond do not decrease monotonically along the series.[17] To our knowledge, only the monoxides have been the object of theoretical studies treating explicitly the relativistic effect, and in PtO both the existence of the filled 4f shell and the relativistic contraction of the s orbital lead to the prediction of a slightly stronger metal−oxygen bond than in NiO. It would thus be interesting to compare the evolution of the bond strength in the dioxide compounds, as our results suggest an even more pronounced effect than in the monoxides.

Acknowledgment. This work was supported by CNRS Grant UMR 7075 and NSF Grant CHE97-00116 and by the University Pierre et Marie Curie via an invited Professorship and the University of Virginia via a Sesquicentennial Associateship for L.A.

References and Notes

(1) Dedieu, A. *Chem. Rev.* **2000**, *100*, 543.
(2) Bauschlicher, C. W., Jr.; Nelin, C. J.; Bagus, P. S. *J. Chem. Phys.* **1985**, *82*, 3265.
(3) Chung. S. C.; Krüger, S.; Pacchioni, G.; Rösch, N. *J. Chem. Phys.* **1995**, *102*, 3695.
(4) Siegbahn, P. E. M. *J. Phys. Chem.* **1993**, *97*, 9096.
(5) Matsui, R.; Senba, K.; Honma, K. *J. Phys. Chem. A* **1997**, *101*, 179.
(6) Wu, H.; Wang, L. S. *J. Chem. Phys.* **1997**, *107*, 17.
(7) Huber, H.; Klotzbücher, W.; Ozin, G. A.; VanVoet, A. *Can. J. Chem.* **1973**, *51*, 2722.
(8) Citra, A. Chertihin, G. V.; Andrews, L.; Neurock, M. *J. Phys. Chem. A* **1997**, *101*, 3109.
(9) Bare, W.; Citra, A.; Chertihin, G. V.; Andrews, L. *J. Phys. Chem. A* **1999**, *103*, 5456.
(10) Andrews, L.; Zhou, M.; Chertihin, G. V.; Bauschlicher, C. W., Jr. *J. Phys. Chem. A*, **2000**, *103*, 6525.
(11) Manceron, L.; Tremblay, B.; Alikhani, M. E. *J. Phys. Chem. A* **2000**, *104*, 3750.
(12) Moore, C. F. *Atomic Energy Levels*; NSRD-NBS; U.S. GPO: Washington, DC, 1971; Vol. III.
(13) Wang, X.; Andrews, L. *J. Phys. Chem. A* **2001**, *105*, 5812.
(14) Schroeder, W.; Grinter. R.; Schrittenlacher, W.; Rotermund. H. H.; Kolb, D. M. *J. Chem. Phys.* **1985**, *82*, 1623.
(15) Blomberg. M. R. A.; Siegbahn, P. E. M.; Strich, A. *Chem. Phys.* **1985**, *97*, 285.
(16) Bauschlicher, C. W., Jr.; Langhoff, S. R.; Partridge, H.; Sodupe, M. *J. Phys. Chem.* **1993**, *97*, 856.
(17) Sunderlin, L. S.; Wang, D.; Squires, R. *J. Am. Chem. Soc.* **1992**, *114*, 2788.